Nanoscale

3D Halos Assembled from Fe3O4/Au NPs with Enhanced Catalytic and Optical Properties

Journal:	*Nanoscale*
Manuscript ID	NR-ART-07-2019-005874.R1
Article Type:	Paper
Date Submitted by the Author:	14-Oct-2019

Complete List of Authors:	Cai, Ren; University of Florida, Chemistry; Nanyang Technological University, Materials Science & Engineering Yang, Dan; Swinburne University of Technology, Centre for Micro-Photonics Lin, Keng-Te; Swinburne University of Technology, Centre for Micro-Photonics Cao, Thai Son ; University of Florida Lv, Yifan; Hunan university, Chen, Kangfu; University of Florida, Mechanical and Aerospace Engineering; University of Florida Yang, Lu; University of Florida Ge, Jia; University of Florida, Chemistry Xia, Lian; University of Florida, Chemistry Christou, George; University of Florida, Department of Chemistry zhao, yuliang; Institute of High Energy Physics, Chinese Academy of Sciences, Chen, Zhuo; Hunan University, State Key Lab of Chemo/Biosensing and Chemometrics Tan, Weihong; P.O Box 117200, University of Florida

Nanoscale

ARTICLE

3D Halos Assembled from Fe_3O_4/Au NPs with Enhanced Catalytic and Optical Properties

Received 00th January 20xx,
Accepted 00th January 20xx

DOI: 10.1039/x0xx00000x

www.rsc.org/

Ren Cai,[a,b⊥] Dan Yang,[d⊥] Keng-Te Lin,[d] Thai Son Cao,[b] Yifan Lyv,[a,c] Kangfu Chen,[f] Yu Yang,[b] Jia Ge,[b] Lian Xia,[b] George Christou,[b] Yuliang Zhao,[e] Zhuo Chen,[a] and Weihong Tan [a,b,c*]

3D structures assembled from multiple components have attracted increasing research interest based on their enriched functionalities and broadened applications. Here, we report a bottom-up strategy to fabricate 3D halos through co-assembly of Fe_3O_4 and Au nanoparticles (NPs). Typically, Fe_3O_4 NPs assemble into a 3D core (size around 500 nm) with simultaneous Au NPs growth on the 3D surface during the assembly process. As a general approach, a variety of 3D halos were fabricated from co-assembly of Fe_3O_4 and Au NPs of different sizes and shapes. To demonstrate the advantages of these 3D halo structures, their catalytic activity to mimic natural enzymes was investigated. Compared with Fe_3O_4 NP building blocks, enhanced catalytic efficiency was achieved by the 3D halos. In addition, the optical behavior of the 3D halos was simulated using a three-dimensional finite-difference time-domain (3D-FDTD) method. As shown in the results, the 3D halos attached to 90 nm Au NPs could absorb more incident light owing to high electric field intensities, making these structures promising for applications in energy harvesting and detection-related fields.

Introduction

Assembly of functional building blocks into novel 3D architectures is highly desirable for a wide range of applications in areas such as catalysis,[1] biomedical diagnosis,[2] sensors,[3] magnetic resonance imaging,[4] plasmonics,[5] and drug delivery.[6] Assembly of nanocrystals into well-defined ordered arrays is one of the most promising techniques to achieve novel materials with advanced functionalities. In the traditional top-down assembly technology, external instrumentation is required to remove or delete substances from large bulk materials to create nano- or micro-sized counterparts in assembled structures. However, large-scale application of this method is hindered by the high cost and size limitation involved in the fabrication process.[7] On the contrary, a bottom-up strategy, which brings together individual inorganic nanocrystals into a well-defined nanostructure through chemical assembly, has proven to be more flexible and efficient.[8,9,10] For instance, Au nanotrucks were assembled via DNA hybridization and used as a photo-controllable drug delivery system for smart cancer therapy.[11] 3D superstructures were assembled from PbS nanocrystals with different sizes through a two-layer phase diffusion technique in vertically positioned glass test tubes.[12] Similarly, a large variety of superstructures were fabricated from self-assembly of micro- and nanoparticles, nanowires, nanosheets, nanocubes and even cells.[13]

More importantly, the research focus in recent years has evolved into assembly of multicomponent nanocrystals with more complex 2D or 3D architectures with the aim of integrating their optical, magnetic, electronic and catalytic properties for broadened practical applications.[14] At the same time, while systematic understanding of the growth processes of these complex aggregates from primary NPs is consequential, the issue has remained understudied. Therefore, we herein report the controllable preparation of 3D halos through bottom-up co-assembly of Au and Fe_3O_4 NPs without any template or substrate. Such design is expected to address the limitation(s) of single-component Fe_3O_4-based devices by

[a] Molecular Sciences and Biomedicine Laboratory, State Key Laboratory for Chemo/Biosensing and Chemometrics, College of Chemistry and Chemical Engineering and College of Biology, Collaborative Innovation Center for Molecular Engineering and Theranostics, Hunan University, Changsha 410082, China. E-mail: tan@chem.ufl.edu
[b] Institute of Molecular Medicine, Renji Hospital, Shanghai Jiao Tong University School of Medicine, and College of Chemistry and Chemical Engineering, Shanghai Jiao Tong University, Shanghai, China
[c] Department of Chemistry and Department of Physiology and Functional Genomics, Center for Research at the Bio/Nano Interface, Shands Cancer Center, UF Genetics Institute, McKnight Brain Institute, University of Florida, Gainesville, FL 32611-7200 (USA) Fax: (+1)352-846-2410.
[d] Centre for Micro-Photonics, Faculty of Science, Engineering and Technology, Swinburne University of Technology, PO Box 218, Hawthorn, Australia
[e] National Center for Nanoscience and Technology, Chinese Academy of Sciences, Beijing 100049, China
[f] Department of Mechanical and Aerospace Engineering, University of Florida, Gainesville, Florida 32611-6250, United States
⊥ R.C. and D.Y. equally contributed to this work.
† Footnotes relating to the title and/or authors should appear here.
Electronic Supplementary Information (ESI) available: Characterization of Fe_3O_4 NPs and Fe_3O_4 NP micelles, Au NPs, hybrid 2D nanosheets functionalized with Au NPs, UV/Vis spectra and photographs (inset) of the catalytic properties of 3D halos with Au NRs using TMB as the substrate in the presence of H_2O_2 (pH 4.5, 25 °C). See DOI: 10.1039/x0xx00000x

programmable integration of Au NPs. Accordingly, Fe_3O_4 NPs typically assemble into the 3D core, and Au NPs with various sizes and shapes (e.g., nanocubes, nanorods, nanotriangles) are dispersed on the surface, forming the so-called "halo" structure, as shown in **Figure 1a**. The complex 3D hetero-structure is generated at increased temperature and can be stably preserved in ethanol and DI water. Thus, instead of simply loading Au NPs on the Fe_3O_4 surface or mixing Au and Fe_3O_4 NPs together, which we have observed in previous studies,[15,16] more rigid binding interaction is generated during this assembly process. The unique design of the 3D halo structure not only brings about enhanced catalytic reactivity towards peroxidase-mimicking as compared to pure Fe_3O_4 NPs, but more importantly, according to our 3D-FDTD simulation, also displays strong and remarkable broad-band absorbance capability from the high electric field intensities attributed by the unique 3D architecture. Consequently, we expect that this architecture would be intriguing for applications in optoelectronics/sensors based on photo-detection or photo-thermal conversion or other related energy-harvesting devices.

Experimental Section

Synthesis of 3D halos: (i) In a typical synthesis of a clear NP-micelle aqueous solution, 30 μL OA was dissolved in a hexane solution of 7-nm Fe_3O_4 NP (1 mg, 0.4 mL) for 15 min. Then, an aqueous solution containing CTAB (100 μL, 20 mg/mL) was added to this mixture. A clear, yellow Fe_3O_4 NP-micelle solution was obtained.

(ii) At the same time, 1 mL 15 nm-Au NPs, 2 mL 40 nm-Au NPs, 2 mL 40 nm-Au NPs mixture, 1 mL 90 nm-Au NPs, and 2 mL Au nanorods (length of ~70 nm) were centrifuged, and the supernatant was discarded, respectively. In each sample, the number of Au NPs was ~ $4x10^{10}$. Then, CTAB solution was added (50 μL, 20 mg/mL).

(iii) Under vigorous stirring, a mixed solvent (3 ml diethylene glycol (DEG) solution containing 100 mg PVP) was quickly added to this Fe_3O_4 NP-micelle solution. The mixture was vortexed for 35 s; then 150 μL of the above Au nanostructures ($4x10^{10}$ Au NPs) were injected and further vortexed for 15 min. Next, the mixture was heated to 85 ^oC and kept for 2 h before the solution was cooled to room temperature. Finally, the resulting products were collected by centrifugation and redispersed in ethanol.

Catalyzed oxidation: Unless otherwise stated, steady state kinetics assays were carried out at 30 ^oC in a 2-mL tube with 0.67 μg 3D halos or Fe_3O_4 NPs in 500 μL reaction buffer (0.2 M NaAc, pH 4.5) in the presence of 530 μM H_2O_2 for 3D halos and Fe_3O_4 NPs, using 800 μM 3,3',5,5'-tetramethylbenzidine (TMB) as the substrate. In a typical experiment, 30 μL H_2O_2 were added to a 430 μL reaction buffer at different pH values at 30 ^oC and vortexed for 3 min. Then, 40 μL TMB (10 mM) were added to the mixture and vortexed for another 3 min. Finally, 0.67 μL of 3D halos (1 mg/mL) was quickly added to the mixture. Immediately after the substrates were added, color changes were observed. All reactions were monitored according to the maximum intensity of absorbance in time-scan mode at 652 nm using a Cary Bio-100 UV/Vis spectrometer (Varian). The final concentration of Fe_3O_4 NPs or NPs in 3D halos was 2.4×10^{-11}M.

Results and discussion

Typically, Fe_3O_4 NPs (size ~ 7 nm, **Figure S1**) with oleic acid (OA) ligands were prepared according to a previously reported method.[17a] Then, an aqueous solution of cetyltri–methylammonium bromide (CTAB) was added to a hexane solution of OA-ligated Fe_3O_4 NPs to form NP micelles by vigorous agitation. Here, CTAB works as a wrapping agent to transfer the hydrophobic NPs to the aqueous phase.[18] Upon addition of CTAB, the Fe_3O_4 NPs adopted an interdigitated bilayer micelle structure with OA ligands as the inner layer and CTAB as the outer layer (**Figure S2**).[7,8] Later, a mixed solvent (of diethylene glycol (DEG) and polyvinylpyrrolidone (PVP)) was injected into the above NP micelles (**Scheme 1a**). To form the halo structure, a solution of Au NRs (lengths of ~70 nm, **Figure S5d**) was injected. Finally, the mixture was heated to 85 ^oC (**Scheme 1b**) and incubated 2 h before the solution was cooled to room temperature. Transmission electron microscopy (TEM) images showed that the as-obtained products were well-dispersed 3D particles with sizes of ~ 500 nm (**Figure 1b**). The enlarged TEM images of typical 3D particles in **Figure 1c-d** revealed their halo-like architecture (hereinafter term "3D halo") in which the 3D core was close-packed by Fe_3O_4 NPs with Au NRs anchored on the core surface. As shown in **Figure 1b** (inset), these halos showed a polycrystalline-like electron diffraction (ED) pattern. To investigate the magnetic properties of this 3D halo structure, the hysteresis measurements for Fe_3O_4 NPs and 3D halos were carried out and are presented in **Figure 2**. The saturation magnetization of 3D halos (~45 emu/g) was lower than that of Fe_3O_4 NPs **(**~52 emu/g) and bulk Fe_3O_4 powder (~90 emu/g)[17b] due to the spin surface effects (**Figure 2**). Furthermore, 3D halos exhibit smaller magnetic coercivities (~250 Oe) than that of Fe_3O_4 NPs (~390 Oe), indicating excellent superparamagnetic behavior of the 3D halos.

Different parameters, such as solvent composition, reaction temperature, type and amount of ligands (PVP, CTAB and OA), were carefully tuned to investigate the key elements determining formation of the 3D halos. More specifically, results show that the correct solvent and temperature are prerequisites for the assembly of the 3D cores. DEG facilitates the assembly process because of its chemical inertness, polarity, and low evaporation rate, as well as the high surface tension, which strongly influences the spreading and assembly of the nanocrystals.[19,20] When ethanol, DI water, Tween-20 and poly (ethylene glycol) 400 were used for the assembly process instead of DEG, no assembled products were generated. Besides, addition of PVP is essential because no assembled product was collected without PVP in the DEG solvent. On the other hand, temperature also influences the self-assembly of 3D cores. The same experimental process was carried out at 45 ^oC, 65 ^oC, 85 ^oC and 100 ^oC, but the 3D core structure could only be collected at 85 ^oC. Under lower temperatures, no assembled products (45 ^oC), or few aggregated products (65 ^oC), were

collected (**Figure S3a**). At higher temperature (100 °C), some irregular 3D structures were observed (**Figure S3b**). It is well known that interparticle interactions (van der Waals force) and ligand repulsive solvo-phobic interactions decide assembled structure.[8,21] During the assembly process, CTAB (outer layer) acts as a cationic surfactant to transfer hydrophobic OA-ligated NPs into hydrophilic solution by a ligand-wrapped reaction,[22] forming Fe_3O_4 NP micelles (**Scheme 1a**). With increased solubility of hydrophilic CTAB in mixed solvent (DEG and PVP) upon heating (**Scheme 1b**), the CTAB layer quickly detaches from NP micelles and leaves OA-capped NPs "wrapped" inside mixed solvent with the assistance of PVP surfactant (**Scheme 1c**).[21,23] Thus, the successful assembly of 3D cores (85 °C, **Figure 1**) results from a balance between the elastic repulsive force of ligands and van der Waals attractive forces.[24,25,26] As shown in **Figure 3a**, naked 3D cores (size around 500 nm) without Au NPs could be formed, just by carefully controlling temperature and solvent.

However, the process described above became more complicated when we tried to manipulate the assembly of both Fe_3O_4 and the Au NPs to form the halo structure. Results showed that formation of the halo structure depends on the amount of OA ligands attached to the NPs surface. For example, without OA, bulk products were formed (**Figure 3b**). In contrast, upon addition of 10 μL OA (3.159×10^3 OA per NP), Fe_3O_4 NPs aggregated to form large and irregular particles, and Au NRs were sparsely dispersed as the outer layer (**Figure 3c**). Well-dispersed 3D halos composed of Fe_3O_4 and Au NRs could be formed only when the amount of OA was increased to 30 μL (9.478×10^3 OA per NP) (**Figure 1**). With further increase of OA to 40 μL (1.264×10^4 OA per NP), the 3D core structure became semi-transparent particle/vesicles (**Figure 3d**).[27] In sum, OA mediates the assembly of Fe_3O_4 NPs to form the 3D core, and Au NRs bind to the 3D core by van der Waals forces and hydrophobic attraction of the hydrophobic groups on the ligands.[28] With excess OA (40 μL, 1.264×10^4 OA per NP), elastic repulsions of ligands are enhanced,[8] and this promotes dispersion of Fe_3O_4 NPs such that the distance between NPs gradually increases, resulting in swelling of the 3D particles (**Figure 3d**) (Please see the analysis of entropy-driven self-assembly in Supporting Information). A similar process was observed by using different assembly times, as shown in **Figure S4**.

Subsequently, by simply changing to Au NPs with different sizes and shapes (**Figure S5**), we designed a series of 3D halos (**Figure 4f**). As shown in **Figure 4a**, Au NPs (~15 nm) would adhere to the surface of the 3D halos, while some Au NP clusters could also be observed. On the other hand, "large" Au NPs (~40 nm) grew on each halo (**Figure 4b** and **Figure 4e**). Interestingly, only one Au NP (~90 nm) could be co-assembled with many Fe_3O_4 NPs to form the 3D halo (**Figure 4c**), which was attributed to the limited contact area between two curved surfaces (3D core and large Au NP (~90 nm)), potentially unable to support several "larger" and "heavier" Au NPs. Furthermore, Au NPs (~40 nm) with various morphologies, i.e., nanorods, nanocubes and triangular nanoprisms, could be grafted on surface of each 3D halo (**Figure 4d-e**). As shown above, this bottom-up method is a general approach for the co-assembly of Fe_3O_4 and Au NPs to prepare 3D halos (**Figure 1a** and **Figure 4f**).

To demonstrate one possible application of the 3D halos, we tested their peroxidase-mimicking activities (**Figure 5**), using 3,3',5,5'-tetramethylbenzidine (TMB) and H_2O_2 as the substrate ($H_2O_2 + TMB \xrightarrow{3D\ halos} H_2O + \text{oxidation of TMB}$). For the first set of experiments, we investigated if the 3D halos (Au NRs) could catalyze the reaction between TMB and H_2O_2. As shown in **Figure S6**, the colorless solution became light blue after about 30 s, and finally turned to deep blue after about 4.5 min, indicating excellent catalytic capability. The experimental pH and temperature for catalysis of 3D halos were 4.5 and 30 °C, respectively, in order to match the optimal values of the natural enzyme horseradish peroxidase (HRP).[29] Except for 3D halos with Au NPs (~90 nm), the data in **Figure 5a-b** and **Figure S7** confirm the maximum initial velocity (V_{max}) of these 3D halos to be around 135% higher than that of their Fe_3O_4 NP building blocks. Catalytic efficiency to substrates, or K_{cat}, is another kinetic parameter.[30] With TMB or H_2O_2 as the substrate, the apparent K_{cat} value is about 35% higher than that of their Fe_3O_4 NP building blocks (**Figure 5c-d**), which have a K_{cat} value about 60% higher than that of HRP,[30] indicating more favorable catalytic properties and enhanced catalytic reactivity, characteristics which would be useful in mimicking HRP. This apparent successful mimicry can be attributed to the collective properties of the building blocks (Fe_3O_4 NPs) and the good distribution of Au NPs on 3D halos, leading to higher catalytic activity and efficiency for TMB and H_2O_2 interaction.[31] Excepting 3D halos with Au NPs (~90 nm) was noted above because they displayed lower catalytic activity resulting from fewer Au NPs and fewer active sites interacting with substrates. Regardless, these results demonstrate that the 3D halos could serve as a better enzyme system for TMB oxidation than Fe_3O_4 NPs or the natural enzyme (HRP).

To investigate the optical properties of 3D halos, we used a 3D-FDTD method to simulate the electric field distributions of the Fe_3O_4/Au (~90 nm) structure at different wavelengths. In the simulation, we set the 3D core (packed by Fe_3O_4 NPs) and a single Au NP to have diameters of 500 nm and 90 nm (**Figure 4c**), respectively, and plane waves with transverse-electric (TE)-polarization propagating from 1 μm above the composite structure in water. All of the optical constants of the materials (Fe_3O_4, Au, and water) were obtained from the literature.[32,33] **Figure 6a-e** display the electric field distributions of incident light at wavelengths of 580 nm, 650 nm, 770 nm, 840 nm, and 940 nm, respectively, passing through the 3D halo structure (Fe_3O_4-Au NPs composite). We found that the 3D halo structure provided strong electric fields within the near field around the Fe_3O_4-Au interface at these wavelengths. Furthermore, the 3D halo structures provided high electric field intensities (IE/E_0I) from the visible (**Figure 6a-c**) to the near-infrared (NIR, **Figure 6d-e**) regions. We attribute these phenomena to the excited surface plasmon polaritons (SPPs) confined in high refractive index material such as treated glass or polymer. The high electric field intensities cause more incident light to be absorbed by the 3D halo structures. In

addition, we investigated the optical properties of the 3D halo structures with distinct dimensions at different wavelengths (for details, please see **Figure S8-S10**). We therefore suggest that the 3D halos can provide good electric field confinement over the visible and NIR range and good energy conversion capability for use in energy harvesting, detection, and biosensing-related applications.

Conclusions

In conclusion, we have developed a bottom-up route to fabricate 3D halos through co-assembly of Au and Fe_3O_4 NPs. As a general approach, Fe_3O_4 and Au NPs of different sizes and shapes can co-assemble into a variety of 3D halos, creating new opportunities to explore assembled materials with enriched functionalities. When used as a catalyst for TMB oxidation, the 3D halos exhibited higher catalytic efficiency compared with Fe_3O_4 NP building blocks, and they demonstrated functional mimicry of the natural enzyme. Moreover, as demonstrated by our simulation process, these 3D halos could absorb more incident light owing to the intensified electrical field from the assembled structure, making them suitable for applications in energy harvesting and detection-related areas. Therefore, the as-developed assembly method can be regarded as a general approach to hybridize noble metal NPs with 3D particles to form functional materials. We believe that this novel method will stimulate the design of multidimensional materials based on a structural design that is similar to that of our 3D halos, thereby expanding the potential applications of such materials in catalysis or optoelectronics/sensors based on photo-detection and photo-thermal conversion.

Acknowledgements

The authors are grateful to Dr Kathryn Williams for her critical comments during the preparation of this manuscript. This work is supported by NSFC grants (NSFC 21521063), and by NIH GM R35 127130 and NSF 1645215.

Notes and references

1 Y. J. Kang, X. C. Ye, J. Chen, L. Qi, R. E. Diaz, V. Doan-Nguyen, G. Z. Xing, C. R. Kagan, J. Li, R. J. Gorte, E. A. Stach, C. B. Murray, *J. Am. Chem. Soc.,* **2013,** *135*, 1499-1505.

2 G. Zhu, R. Hu, Z. Zhao, Z. Chen, X. Zhang, W. Tan, *J. Am. Chem. Soc.,* **2013,** *135*, 16438-16445.

3 a) J. B. Liu, S. H. Fu, B. Yuan, Y. L. Li, Z. X. Deng, *J. Am. Chem. Soc.,* **2010,** *132*, 7279-7281; b) W. Ma, P. Fu, M. Sun, L. Xu, H. Kuang, C. Xu, *J. Am. Chem. Soc.,* **2017,** *139*, 11752-11759; c) A. Qu, M. Sun, L. Xu, C. Hao, X. Wu, C. Xu, N. A. Kotov, H. Kuang, *Proc. Natl. Acad. Sci. U. S. A.* **2019,** *116*, 3391-3400.

4 O. Chen, L. Riedemann, F. Etoc, H. Herrmann, M. Coppey, M. Barch, C. T. Farrar, J. Zhao, O. T. Bruns, H. Wei, P. Guo, J. Cui, R. Jensen, Y. Chen, D. K. Harris, J. M. Cordero, Z. Wang, A. Jasanoff, D. Fukumura, R. Reimer, M. Dahan, R. K. Jain, M. G. Bawendi, *Nat. Commun.,* **2014,** *5*.

5 H. Chen, L. Shao, Q. Li, J. Wang, *Chem. Soc. Rev.,* **2013,** *42*, 2679-2724.

6 L. Y. T. Chou, K. Zagorovsky, W. C. W. Chan, *Nat. Nanotechnol.,* **2014,** *9*, 148-155.

7 N. Vogel, M. Retsch, C. A. Fustin, A. del Campo, U. Jonas, *Chem. Rev.,* **2015,** *115*, 6265-6311.

8 M. A. Boles, M. Engel, D. V. Talapin, *Chem. Rev.,* **2016**, *116*, 11220-11289.

9 E. Auyeung, T. I. N. G. Li, A. J. Senesi, A. L. Schmucker, B. C. Pals, M. O. de la Cruz, C. A. Mirkin, *Nature* **2013,** *505*, 733.

10 R. J. Macfarlane, B. Lee, M. R. Jones, N. Harris, G. C. Schatz, C. A. Mirkin, *Science* **2011,** *334*, 204-208.

11 L. Qiu, T. Chen, I. Öçsoy, E. Yasun, C. Wu, G. Zhu, M. You, D. Han, J. Jiang, R. Yu, W. Tan, *Nano Lett.,* **2015,** *15*, 457-46.

12 S. M. Rupich, E. V. Shevchenko, M. I. Bodnarchuk, B. Lee, D. V. Talapin, *J. Am. Chem. Soc.,* **2010,** *132*, 289-296.

13 J. Guo, B. L. Tardy, A. J. Christofferson, Y. Dai, J. J. Richardson, W. Zhu, M. Hu, Y. Ju, J. Cui, R. R. Dagastine, I. Yarovsky, F. Caruso, *Nat. Nanotechnol.* **2016,** *11*, 1105-1111.

14 K. Miszta, J. de Graaf, G. Bertoni, D. Dorfs, R. Brescia, S. Marras, L. Ceseracciu, R. Cingolani, R. van Roij, M. Dijkstra, L. Manna, *Nat. Mater.,* **2011,** *10*, 872-876.

15 Y. Xiang, H. Yang, X. Guo, Y. Wu, Y. Ying, Y. Wen, H. Yang, *Microchim. Acta* **2018,** *185*, 195.

16 S. Villa, P. Riani, F. Locardi, F. Canepa, *Materials (Basel)* **2016,** *9*, 826

17 (a) Y. Li, F. Ma, X. Su, C. Sun, J. Liu, Z. Sun, Y. Hou, *Catal. Commun.,* **2012,** *26*, 231-234; (b) H. Iida, K. Takayanagi, T. Nakanishi, T. Osaka. J. Colloid Interface Sci. **2007**, *314*, 274-280.

18 D. V. Talapin, *ACS Nano* **2008,** *2*, 1097-1100.

19 V. Aleksandrovic, D. Greshnykh, I. Randjelovic, A. Frömsdorf, A. Kornowski, S. V. Roth, C. Klinke, H. Weller, *ACS Nano* **2008,** *2*, 1123-1130.

20 Z. Yang, T. Altantzis, D. Zanaga, S. Bals, G. V. Tendeloo, M.-P. Pileni, *J. Am. Chem. Soc.,* **2016,** *138*, 3493-3500.

21 R. Cai, D. Yang, L. Yan, F. Tian, J. Zhang, Y. Lyu, K. Chen, C. Hong, X. Chen, Y. Zhao, Z. Chen, W. Tan, *ACS App. Nano Mater.,* **2018,** *1*, 5389-5395.

22 R. Cai, Y. Du, D. Yang, G. Jia, B. Zhu, B. Chen, Y. Lv, K. Chen, D. Chen, W. Chen, L. Yang, Z. Chen, W. Tan, *Nanoscale*, **2019,** *11*, 12169-12176.

23 M. Grzelczak, J. Vermant, E. M. Furst, L. M. Liz-Marzán, *ACS Nano* **2010,** *4*, 3591-3605.

24 P. Jenkins, M. Snowden, *Adv. Colloid Interface Sci.,* **1996,** *68*, 57-96.

25 K. L. Young, M. R. Jones, J. Zhang, R. J. Macfarlane, R. Esquivel-Sirvent, R. J. Nap, J. Wu, G. C. Schatz, B. Lee, C. A. Mirkin, *Proc. Natl. Acad. Sci. U.S.A.,* **2012,** *109*, 2240-2245.

26 L. Gao, J. Zhuang, L. Nie, J. Zhang, Y. Zhang, N. Gu, T. Wang, J. Feng, D. Yang, S. Perrett, X. Yan, *Nat. Nanotechnol.,* **2007,** *2*, 577-583.

27 R. Cai, D. Yang, K.-T. Lin, Y. Lyu, B. Zhu, Z. He, L. Zhang, Y. Kitamura, L. Qiu, X. Chen, Y. Zhao, Z. Chen and W. Tan, J. *Am. Chem. Soc.*, **2019**, 141, 1725 -1734.

28 Y. Guo, L. Deng, J. Li, S. Guo, E. Wang, S. Dong, *ACS Nano* **2011,** *5*, 1282-1290.

29 R. Cai, D. Yang, S. Peng, X. Chen, Y. Huang, Y. Liu, W. Hou, S. Yang, Z. Liu, W. Tan, *J. Am. Chem. Soc.,* **2015,** *137*, 13957-13963.

30 E. D. Palik, Handbook of Optical Constants of Solids, Academic Press: San Diego, 1998.

31 P. B. Johnson, R. W. Christy, *Phys. Rev. B* **1972,** *6*, 4370-4379.

32 L. Luo, C. Ge, Y. Tao, L. Zhu, K. Zheng, W. Wang, Y. Sun, F. Shen, Z. Guo, In *Nanophotonics*, **2016,** 5, 139-146.

Figures and caption

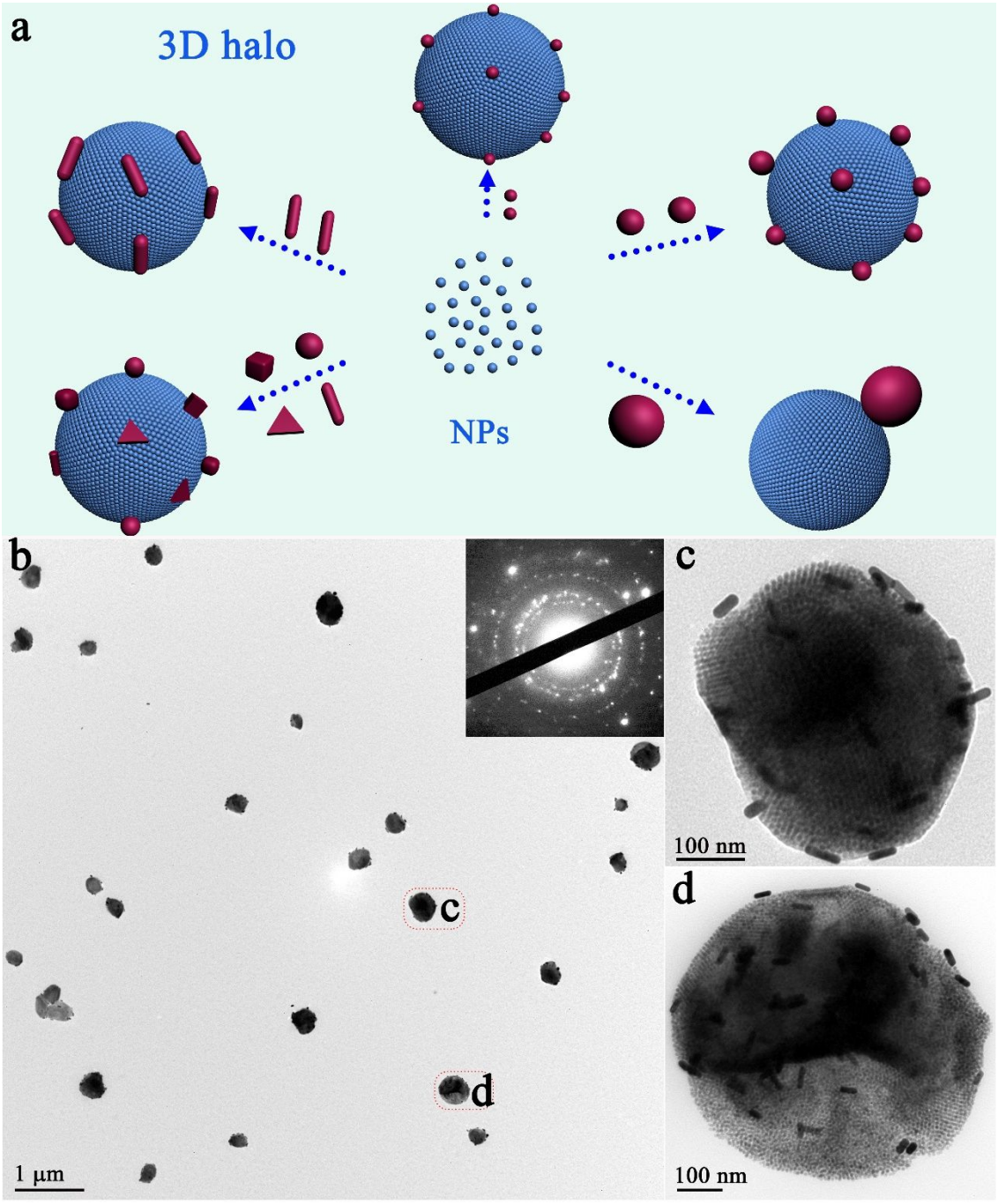

Figure 1 a) scheme for the formation of 3D halos from NP self-assembly; TEM images of 3D halos with Au NRs (length of ~70 nm): b) low-magnification and electron diffraction pattern (inset); c) and d) high-magnification TEM images. Volume of OA is 30 μL.

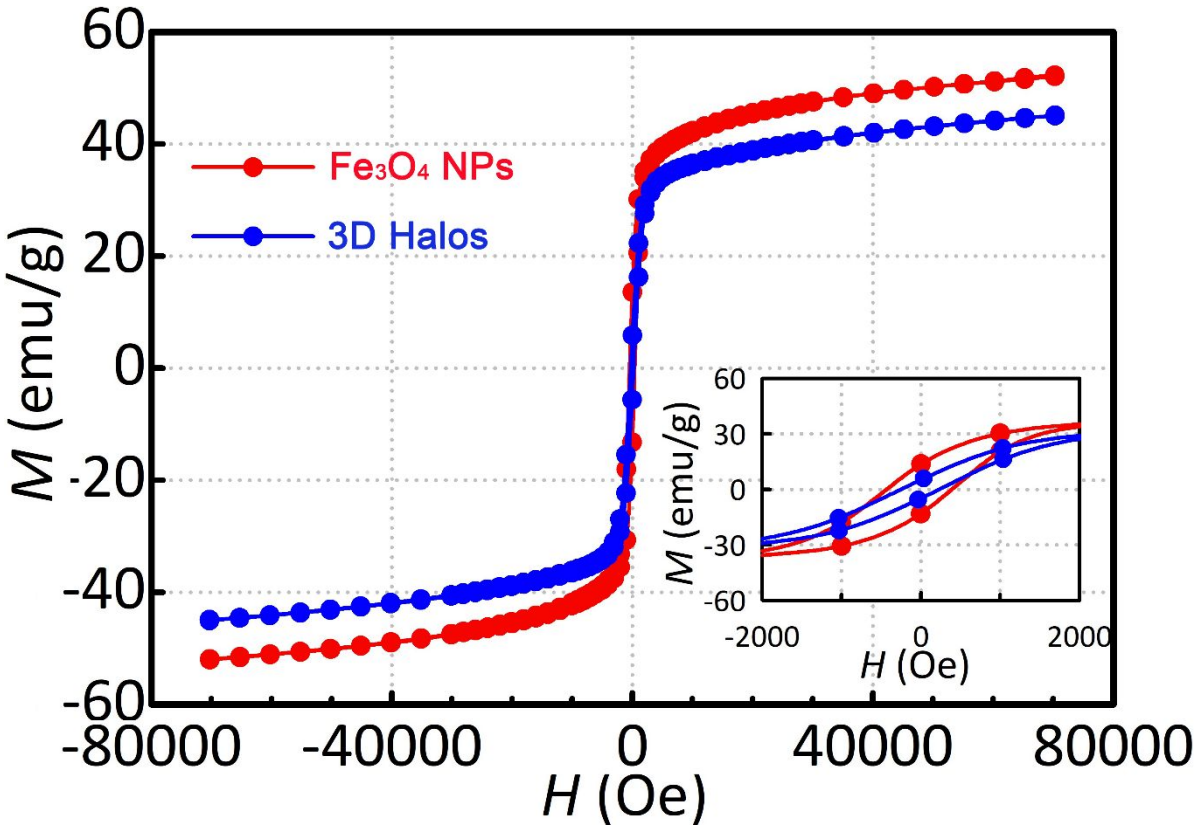

Figure 2 Hysteresis measurements for 3D halos and Fe_3O_4 NPs at 10 K. The inset is data from -2000 to 2000 Oe.

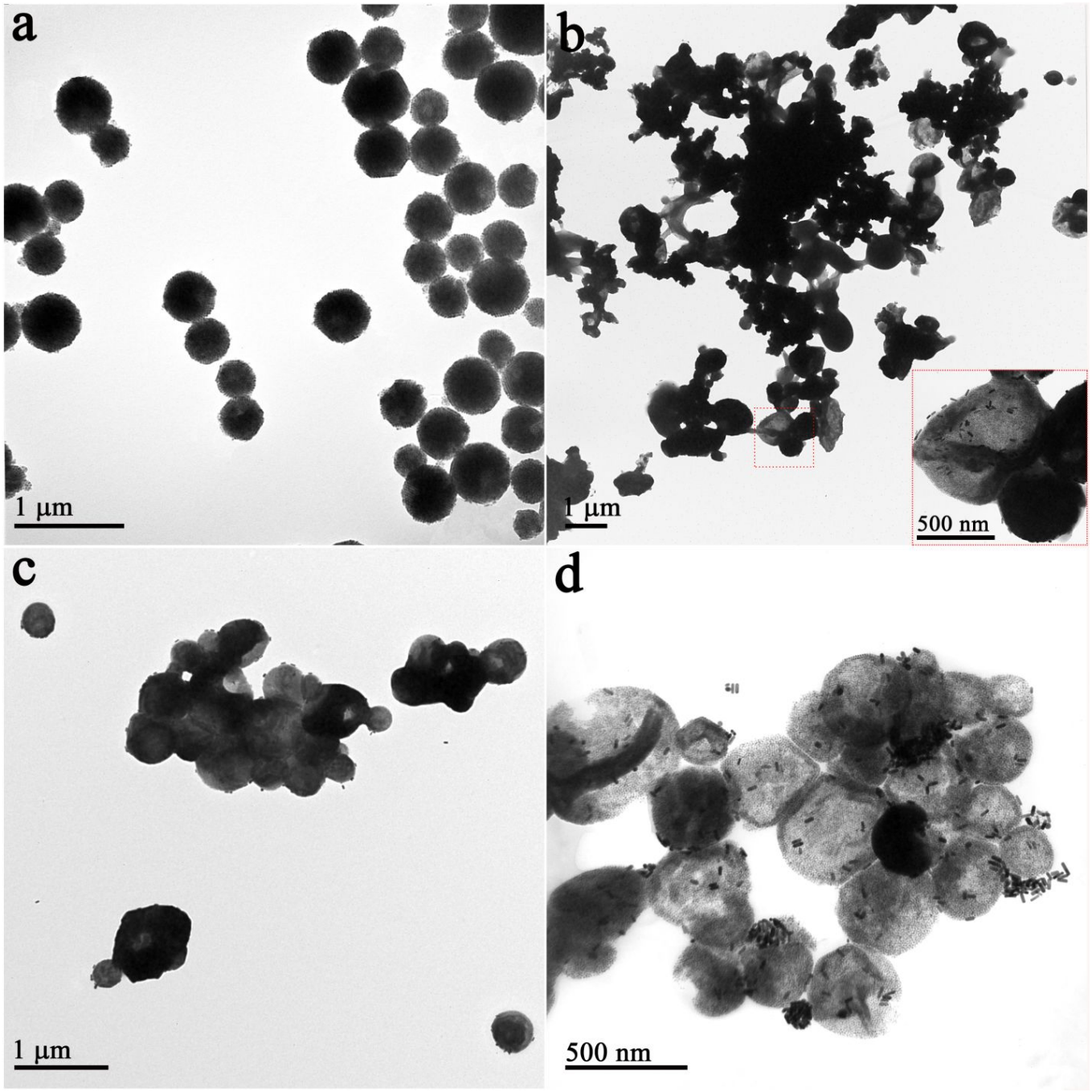

Figure 3 TEM images of intermediate products in the assembly process. The samples prepared from NP self-assembly (Fe_3O_4 NPs and Au NRs) by adding different amounts of OA to stabilize Fe_3O_4 NPs: a) 30μL OA without Au NRs; b) 0 μL OA; c) 10 μL OA; d) 40 μL OA.

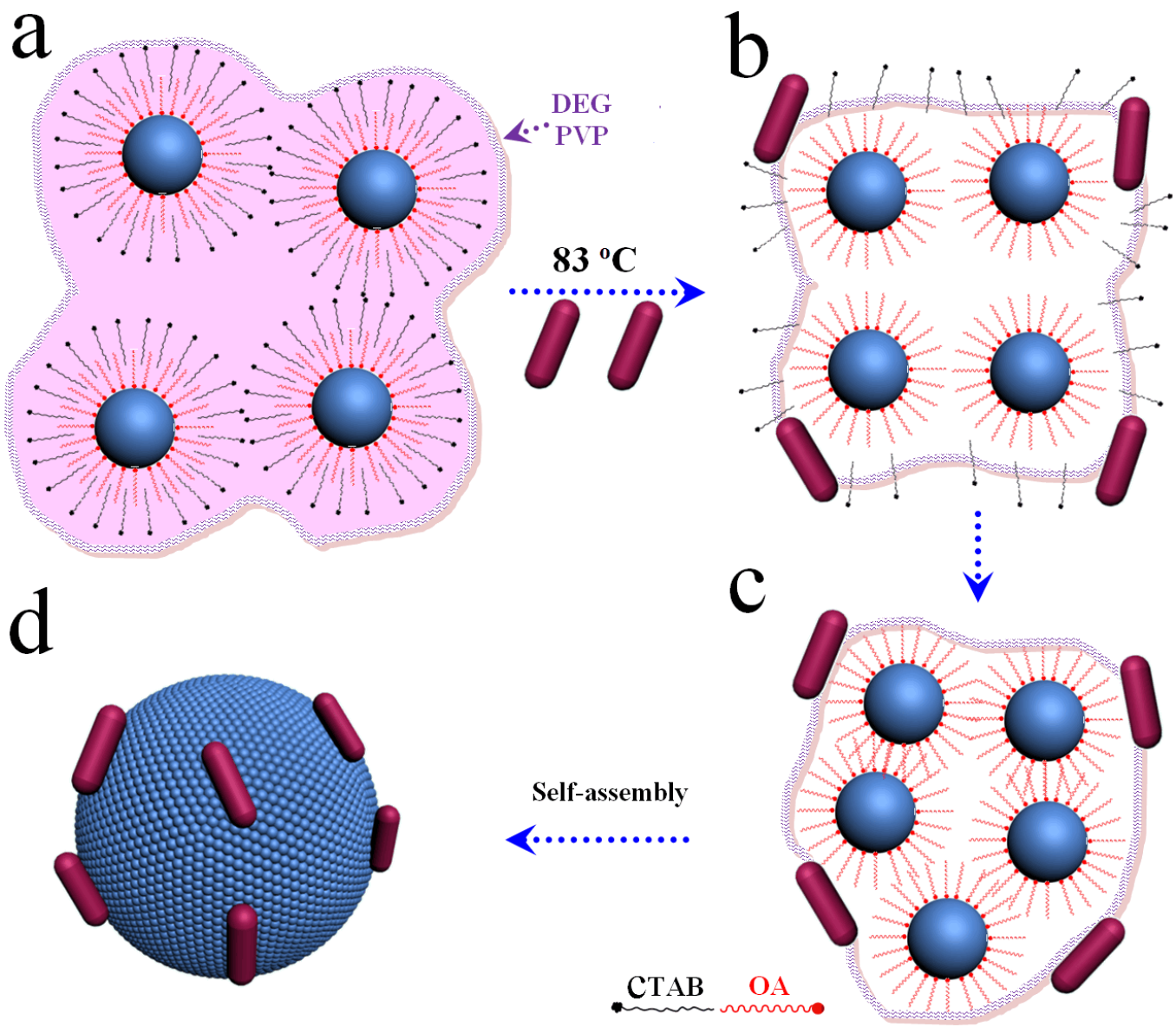

Scheme 1 Scheme for the synthesis of 3D halos by NP self-assembly: a) Fe_3O_4 NP-micelles in DEG; b) self-dissociation of the CTAB layer; c) OA guides NPs rearrangement; d) formation of 3D halos (OA amount is 30 μL).

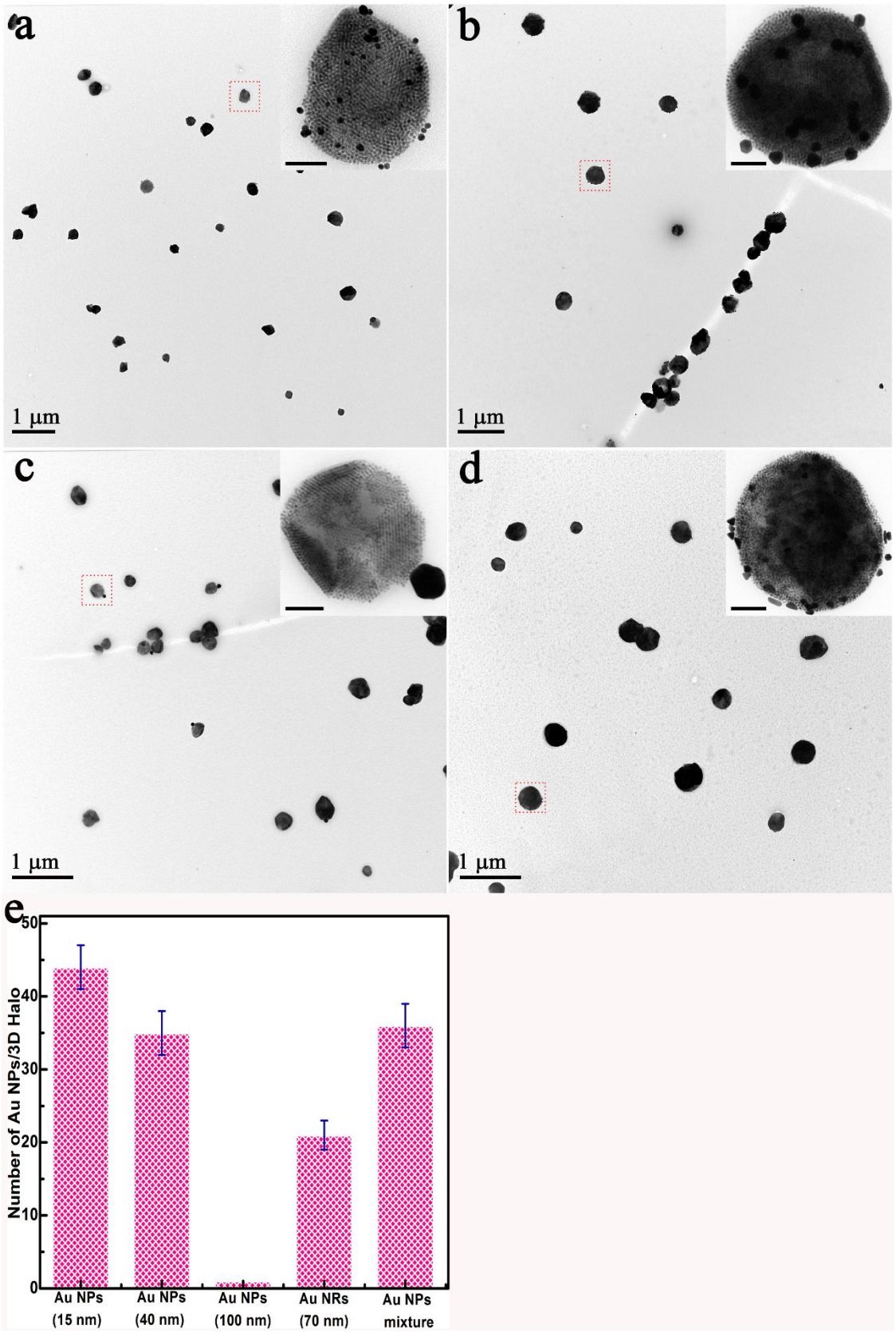

Figure 4 TEM images of 3D halos with different Au NPs: a) Au NPs (~15 nm); b) Au NPs (~40 nm); c) Au NPs (~90 nm); d) Au NP mixture (~ 40 nm) (scale bars are 100 nm in inset images). e) Statistical analysis for average number of Au NPs per 3D halo.

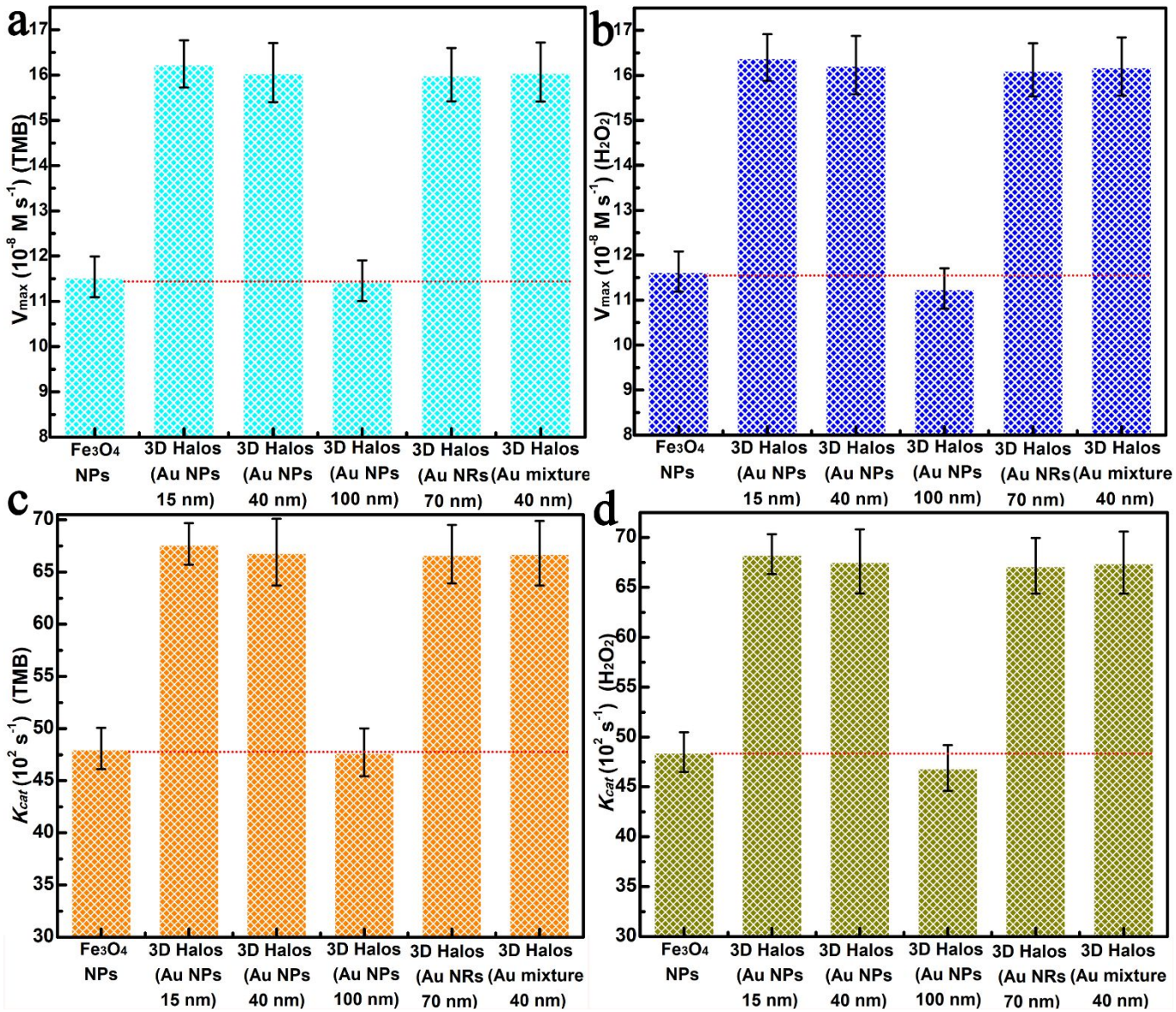

Figure 5 Maximum initial velocity (V_{max}) was measured using Fe_3O_4 NPs and 3D halos: a) concentration of H_2O_2 was 530 μM, and TMB concentration was varied; b) concentration of TMB was 800 μM, and H_2O_2 concentration was varied. The catalytic constant (K_{cat}): c) concentration of H_2O_2 was 530 μM, and TMB concentration was varied; d) concentration of TMB was 800 μM, and H_2O_2 concentration was varied. $K_{cat} = V_{max}/[E]$, where [E] is the enzyme (or NP) concentration (2.4 x 10^{-11} M), and K_{cat} is the maximum number of substrate molecules converted to product per enzyme molecule per second.

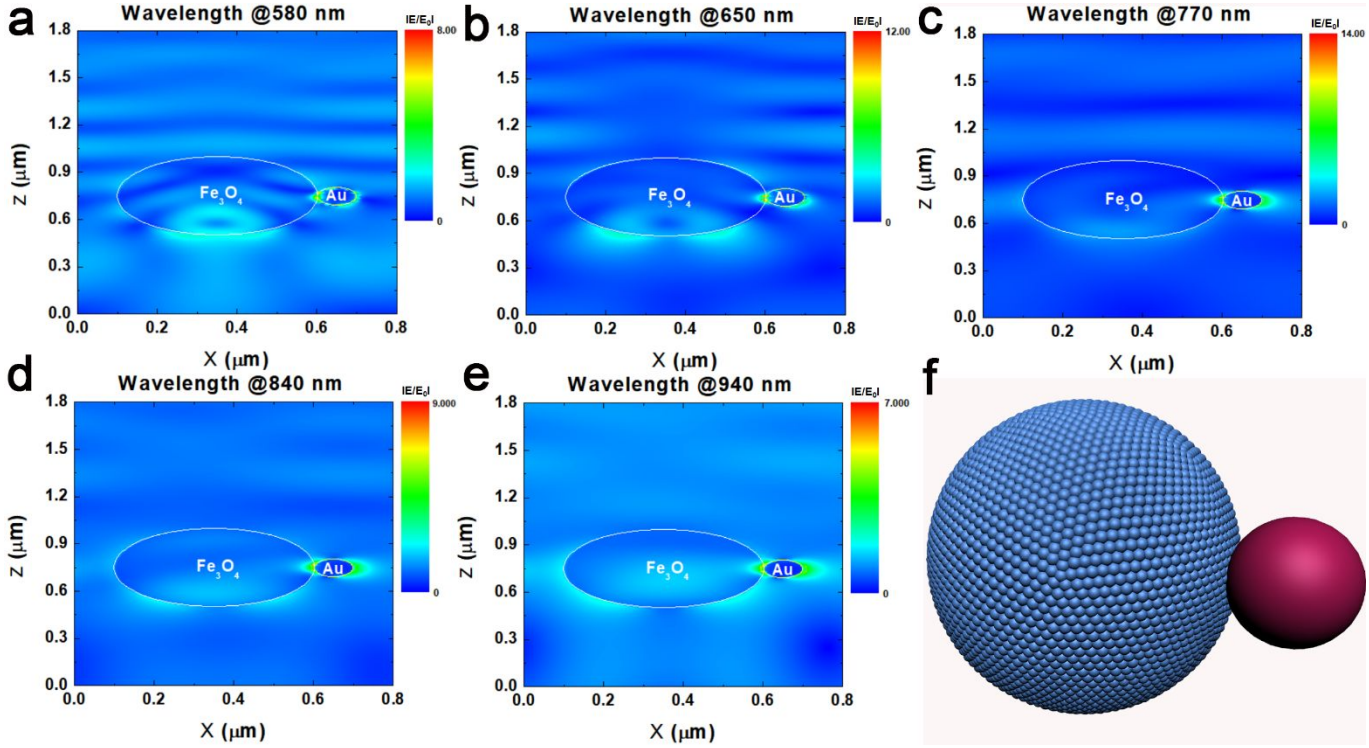

Figure 6 Near-field electric field distributions of incident light at wavelengths of (a) 580 nm; (b) 650 nm; (c) 770 nm; (d) 840 nm; and (e) 940 nm passing through the Fe_3O_4-Au NPs halo structure (f) in water.

Table of contents